Available online at www.sciencedirect.com

ScienceDirect

Procedia Engineering 100 (2015) 115 – 124

Procedia Engineering

www.elsevier.com/locate/procedia

25th DAAAM International Symposium on Intelligent Manufacturing and Automation, DAAAM 2014

Computational Modeling and Simulation of Nonisothermal Free-Surface Flow of a Liquid Jet Impinging on a Heated Surface

Berberović Edin[a], Šikalo Šefko[b,*]

[a] *Polytechnic Faculty, University of Zenica, Fakultetska 1, 72000 Zenica, B&H*
[b] *Faculty of Mechanical Engineering, University of Sarajevo, Vilsonovo Setaliste 9, 71000 Sarajevo, B&H*

Abstract

The study is aimed at formulating and validating the computational model for the nonisothermal two-phase flow with free-surfaces. The testing flow configuration consists of the liquid jet impacting on a heated wall generating simultaneous heat transfer from the wall surface. The interface capturing methodology implemented in the open-source software OpenFOAM® based on the volume-of-fluid (VOF) model in the framework of Computational Fluid Dynamics (CFD) is extended to incorporate heat transfer. The potential of the model is evaluated by contrasting the results of numerical simulations to the existing experimental and numerical results. The computational procedure based on the numerical model demonstrates good qualitative and quantitative predictive capabilities by reproducing correctly the studied flow and heat transfer characteristics.

Peer-review under responsibility of DAAAM International Vienna

Keywords: volume-of-fluid; nonisothermal two-phase flow; numerical simulation; free surface; impinging jet

1. Introduction

Investigation of heat transfer during impingement of liquid jets is of interest in engineering since the thin liquid layer formed by spreading the liquid after the impact enhances heat transfer rates. In the process industry equipment is used that often requires high rates of heat removal from solid surfaces to a liquid which depends on the manner in which heat is transferred from the surface [1]. Heat transfer from a hot surface by wetting it with liquid represents an enhanced way of cooling. In such technologies the nonisothermal flow generated by the jet impact and liquid spreading represents the core of the underlying physical process. The fluid flow developed by a liquid jet impacting on a hot surface represents a complex physical problem governed by various interacting parameters, e.g. jet diameter and velocity, surface temperature and roughness, liquid properties including surface tension. The flow becomes even more difficult to understand when phase change is present. The small scales and high velocities involved in such

Peer-review under responsibility of DAAAM International Vienna
doi:10.1016/j.proeng.2015.01.349

flows inhibit direct experimental access to the phenomena, which is the reason why numerical simulations are receiving more attention. In the present paper the computational model for such a nonisothermal flow is formulated and validated within the framework of the volume-of-fluid-based (VOF) method for free-surface capturing [2]. Due to its relevance in many fields in engineering and industry, interfacial multiphase flow modeling has been the subject of various investigations regarding impingement of liquid jet, droplet impact on surfaces, rising gas bubbles, flow in thin liquid sheets, atomization and some of the more recent contributions are given in [3,4,5,6,7].

From the numerical point of view one of the major difficulties in the VOF method is ensuring the transport of sharply defined interfaces without numerical diffusion. The distribution of the phase fraction is such that the free surface is commonly smeared over a few mesh cells. In common solution methods the free surface is explicitly geometrically reconstructed followed by an advection algorithm. Such methods are suitable mainly for two-dimensional problems and the phase interface is represented as a series of piecewise line segments. The problem reduces to finding the corresponding normal vector to the interface using the known distribution of the phase fraction and reconstructing a line that exactly matches the computed phase fraction values in each interface-containing cell. Once the interface is reconstructed, it is advected by the underlying flow field along the coordinate directions in subsequent separate one-dimensional steps [8,9,10,11]. One of the drawbacks of such methods is that separate one-dimensional advection steps make the advected volume fluxes dependent on which order of coordinate directions is used for the advection and thus errors in mass conservation may arise which may lead to inconsistent phase fraction field.

Contrary to the geometric reconstruction algorithms, volume fluxes can also be determined algebraically, without explicit interface reconstruction, by using a differencing scheme for a proper evaluation of convection fluxes at cell-faces. Some of the previously reported algebraic algorithms are given in [12]. The computational model used in this paper does not reconstruct the phase interface explicitly but uses an algebraic formulation for the calculation of convection fluxes producing bounded and sharp solution. In order to preserve boundedness and prevent smearing of the sharp interfaces, a differencing scheme is designed by a suitable combination of the upwind and downwind differencing. Such combination is referred to as compressive scheme to indicate the ability to sharpen smeared free surface profiles. In addition to requiring less computational time, since there is no unnecessary interface reconstruction, another advantage of the model is that it is more suitable and easy extendable to three-dimensional flow problems.

2. Governing equations

The details of the hydrodynamic model for interface capturing are given in [13]. Here the extension of the model is presented to enable the calculation of heat transfer as well. The mathematical formulation of the nonisothermal free-surface flow includes interface capturing methodology extended to incorporate heat transfer. The governing transport equations are the conservation of mass, phase fraction, momentum and energy

$$\nabla \cdot \mathbf{U} = 0 \tag{1}$$

$$\frac{\partial \gamma}{\partial t} + \nabla \cdot \left(\mathbf{U} \gamma \right) + \nabla \cdot \left[\mathbf{U}_c \gamma \left(1 - \gamma \right) \right] = 0 \tag{2}$$

$$\frac{\partial \left(\rho \mathbf{U} \right)}{\partial t} + \nabla \cdot \left(\rho \mathbf{U} \mathbf{U} \right) = -\nabla p_d - \mathbf{g} \cdot \mathbf{x} \nabla \rho + \nabla \mathbf{T} + \sigma \kappa \nabla \gamma \tag{3}$$

$$\frac{\partial \left(\rho c_p T \right)}{\partial t} + \nabla \cdot \left(\rho c_p \mathbf{U} T \right) = \nabla \cdot \left(k \nabla T \right). \tag{4}$$

The symbols in the governing equations are as follows: $\mathbf{U}$ is the velocity, γ is the liquid volume fraction, $\mathbf{U_c}$ is the compression velocity, ρ is the density, p_d is the modified pressure, $\mathbf{g}$ is the acceleration due to gravity, $\mathbf{x}$ is the

position vector, $\mathbf{T}$ is the viscous stress tensor $\mathbf{T} = \mu[\nabla\mathbf{U} + (\nabla\mathbf{U})^{\mathrm{T}}]$, σ is the surface tension coefficient, κ is the mean surface curvature, c_p is the specific heat, k is the thermal conductivity and T is the temperature, respectively.

The fluid in the model is treated as effective and represents a homogeneous mixture of air and water, both Newtonian immiscible fluids. The properties of the effective fluid are determined as weighted averages based on the phase fraction distribution. Body force due to effects of the surface tension is accounted for by the formulation of the Continuum Surface Force model (CSF) [14] and spatial variation of surface tension is neglected. The term with the density gradient stems from the fact that the modified pressure is defined as $p_d = p - \rho\mathbf{g}\cdot\mathbf{x}$. The position of the free surface is determined from the solution of the transport equation for phase fraction having values between zero and one corresponding to gas and liquid. The transport equation for energy is formulated in the form of the temperature equation where the heat source term from the viscous dissipation is neglected due to small Eckert number in inertia dominated flows, $\mathrm{Eck} = U^2/(c_p\Delta T) << 1$.

The temperature dependence of the density and specific heat of water is very weak in smaller temperature ranges and is therefore neglected. The dependence of the thermophysical properties of air on temperature is also neglected due to the fact that flow and energy balances are determined predominantly by properties of the liquid and the solid substrate. However, the viscosity, thermal conductivity and surface tension of water are treated as temperature dependent according to the following expressions obtained by regression of the available property data from [15,16]:

$$\nu_l = -2.61\cdot10^{-12}T^3 + 5.82\cdot10^{-10}T^2 - 4.68\cdot10^{-8}T^1 + 1.74\cdot10^{-6} \tag{5}$$

$$k_l = -9.74\cdot10^{-6}T^2 + 2.12\cdot10^{-3}T + 5.58\cdot10^{-1} \tag{6}$$

$$\sigma_l = -1.68\cdot10^{-4}T + 7.60\cdot10^{-2}. \tag{7}$$

3. Numerical procedure and computational details

Numerical simulations were carried out using OpenFOAM® (Open Field Operation and Manipulation) CFD Toolbox, an open-source software distributed by the OpenFOAM Foundation. The code is written in the object-oriented manner suitable for solving computational continuum mechanics problems (CCM) [17] and in particular CFD as an established solution methodology in industrial problems [18,19]. The phase fraction γ is in reality a discontinuous function, due to its gradient being non-zero only in the extremely thin region of the interface; however it changes smoothly over the interface in the model yielding a smooth change of the fluid properties and surface tension force. The smearing of steep gradients is suppressed by the additional convective term in the phase fraction equation which introduces a counter-gradient transport against the numerical diffusion and compresses the interface.

The flow and energy equations are solved in a coupled fashion. The solution procedure incorporates an outer iteration loop in every time step, solving iteratively the fluid motion and the energy equation. Fluid properties are updated after each time step and are determined by the calculated phase fraction distribution. The numerical procedure incorporates a cell-center-based finite volume method with finite volume approximation of the transport equations. The unsteady terms are evaluated using the Euler implicit discretization scheme and the terms with spatial derivatives, i.e. convection terms, are integrated over cell surfaces with the cell face values of dependent variables determined by the Van Leer flux limiter [20]. The time step size is self-adjusted during computations using the prescribed Courant number value less than one as a limit. The pressure is coupled with velocity by the Pressure Implicit with Splitting of Operators (PISO) algorithm [21].

The sketch of the flow configuration and the numerical mesh are depicted in Fig. 1. For a better computational efficiency the numerical mesh is two-dimensional axisymmetric slice refined in the regions covering the falling jet and the spreading film, having in total 210000 cells.

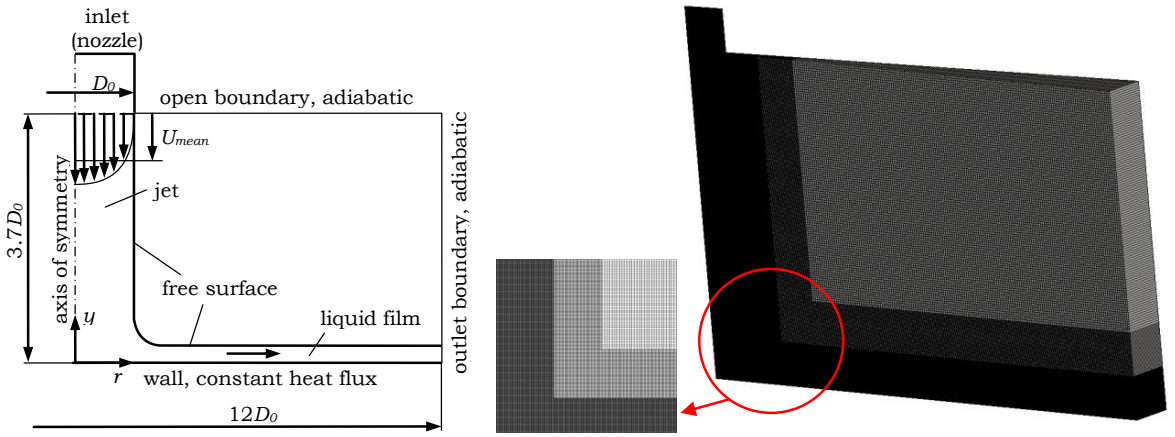

Fig. 1. The water jet impingement case configuration (left) and the numerical mesh (right).

The fluid properties correspond to those of water and air at ambient conditions. The relevant geometrical parameters are the jet diameter D_0 = 4.06 mm, the plate diameter equal to $12D_0$ and the height between the plate and the nozzle outlet of $3.7D_0$. The characteristic Reynolds number based on the mean water velocity at the nozzle exit equals $\mathrm{Re} = D_0 U_{mean}/\nu = 10600$. At the plate surface the constant heat flux $q_w = 1.49 \cdot 10^5$ W/m^2 is applied. Although turbulent flow could be expected at the nozzle exit, its effects were neglected since the radial velocity of the thin liquid film spreading over the heated surface is relatively small and therefore it is assumed that the flow relaminarizes and stays laminar after the impingement.

The simulation is initialized by prescribing the phase fraction distribution equal to unity at the nozzle exit and zero elsewhere. A homogeneous temperature distribution throughout the fluid is prescribed at initial time instant. The boundary conditions consist of the no-slip wall boundary for the substrate and other boundaries being open with prescribed pressure and a combination of inlet and outlet conditions for velocity. At the wall boundary a constant heat flux is applied and at open boundaries adiabatic condition is assumed with zero gradient for the temperature.

4. Results and discussion

The computational algorithm for the nonisothermal two-phase flow with free surface is validated using the case of a liquid jet impinging on a heated surface by comparing the computed results with the empirical results in [22], the numerical results in [23,24] and the experimental results in Stevens [25]. The water jet enters the computational domain through the nozzle and then impinges on the heated plate below. After impingement a thin water sheet is formed flowing over the wall and removing heat from the surface. After the steady state has been reached distributions of the temperature and the heat flux at the wall are established characterized by the wall Nusselt number. The simulations were performed using two different velocity profiles at the nozzle exit: the uniform velocity with $U_y = -U_{mean}$ and the 1/7th power-law profile $U_y = -U_{max}(1 - r/R_0)^{1/7}$, $U_{max} = U_{mean}/0.817$ and $R_0 = D_0/2$.

For the constant applied wall heat flux the conservation of energy requires the fluxes due to heat conduction and convection at the wall surface to be equal

$$q_w = h\left(T_w - T_{ref}\right) = -k_w \nabla T_w\big|_{\perp} \tag{8}$$

where T_{ref} refers to the reference temperature of the undisturbed flow which in this case is the water temperature at the nozzle outlet, and h is the heat transfer coefficient.

The discretization of the convective term in the energy equation requires the values for the temperature at all boundary cell-faces. This is achieved by first calculating the surface-normal temperature gradient from the prescribed wall heat flux and the wall boundary temperature is then obtained by interpolating the cell-center value using the calculated temperature gradient.

Taking the nozzle diameter as the characteristic length, the characteristic Nusselt number for the heat transfer from the wall surface is by definition

$$Nu = \frac{hD_0}{k} = \frac{D_0}{k_w} \frac{q_w}{T_w - T_{ref}}. \tag{9}$$

The computationally obtained normalized positions of the free-surface of the water jet and the film are plotted in Fig. 2 after steady state has been reached for the cases with the uniform and the power-law inlet velocity profiles (velocity profiles at the nozzle outlet).

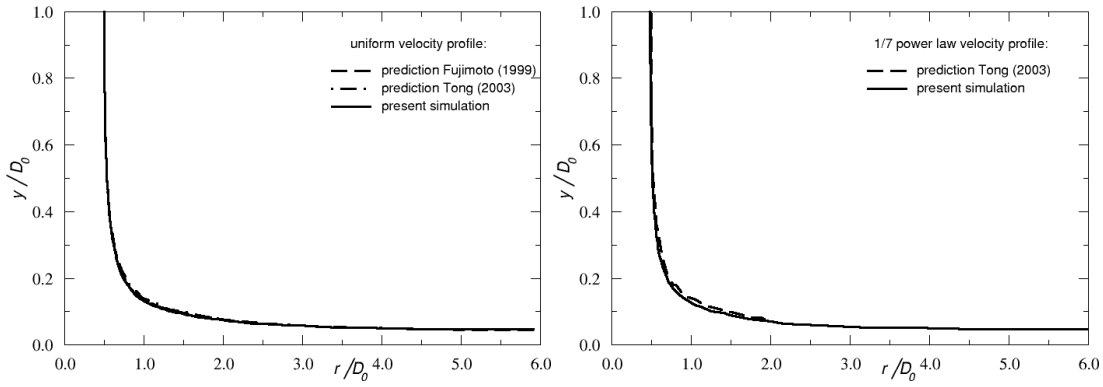

Fig. 2. The position of the free-surface for the uniform (left) and the power-law (right) inlet velocity profile.

Fig. 3. shows the computationally obtained radial dimensionless pressure distributions at the surface of impingement for both velocity profiles at the nozzle outlet, plotted against the normalized radial coordinate (r/D_0). The pressure is made dimensionless by dividing its values with the pressure in the stagnation region p_{stag}, which is the pressure at the wall (cell-face) in the first boundary cell near the axis of symmetry.

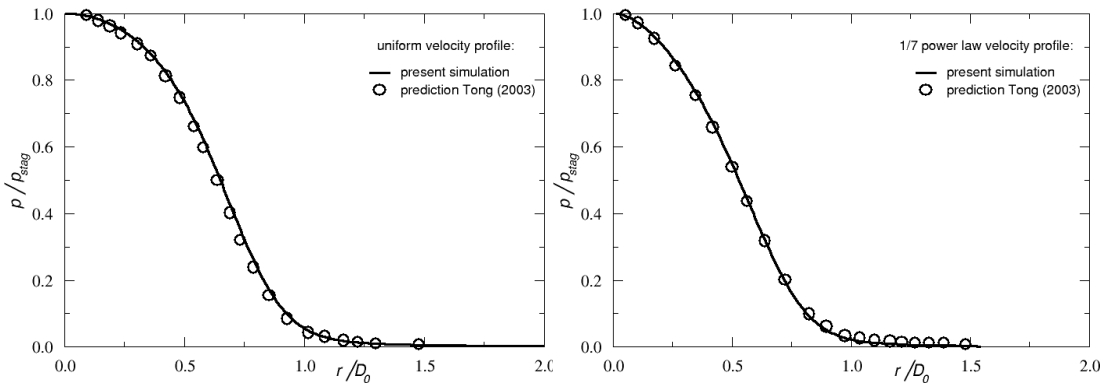

Fig. 3. The dimensionless pressure distribution at the wall for the uniform (left) and the power-law (right) inlet velocity profile.

As can be seen in Fig. 2 and Fig. 3, both, the obtained free-surface positions and the pressure distributions show a very good agreement in comparison to the aforementioned existing numerical results. This indicates that the interface capturing methodology used in the present study is capable of representing the hydrodynamics of the flow correctly. Moreover, due to the large enough distance of the inlet nozzle from the wall beneath, both inlet velocity profiles used in the study yield similar results.

The computationally obtained distributions of the Nusselt number for the two cases are plotted in Fig. 4 for both velocity profiles at the nozzle outlet, plotted against the normalized radial coordinate (r/D_0) and compared to the aforementioned experimental, theoretical and numerical results. In accordance with the previous findings the best agreement with the experimental results was obtained in the case of the uniform velocity profile. In addition in both cases small waves are resolved at the free surface of the spreading water film which is more pronounced in the case of the power-law velocity profile. This explains why the distribution of the Nusselt number shows small oscillations along the normalized radial coordinate in Fig. 2. Some discrepancy in the results for the Nusselt number is observed in the impact region which may be attributed to the fact that the flow in the present study is considered as being laminar while in reality some turbulent motions with higher velocity gradients may be expected to influence the overall heat transfer coefficient.

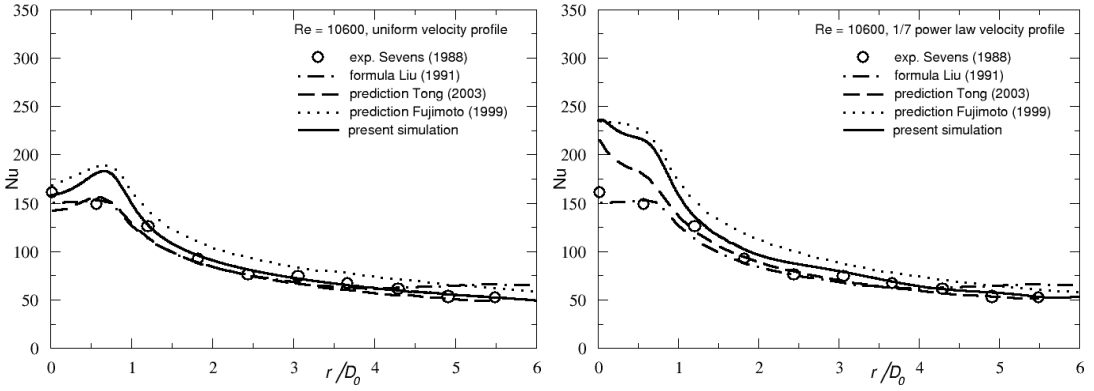

Fig. 4. The Nusselt number distribution at the wall for the uniform (left) and the power-law (right) inlet velocity profile.

The computationally obtained temporal evolution of the flow of the impinging water jet is shown in Fig. 5. The snapshots are taken for the case with the power-law velocity profile at times t = 0, 0.004, 0.008, 0.012, 0.016, 0.022 μs, ordered from top to bottom in two columns. The hydrodynamic development of the flow is such that after the jet impinges on the solid surface it starts spreading radially over the surface and away from the stagnation region in according with the previous results. The stagnation region is formed around the axis of symmetry followed by the development of the velocity and thermal boundary layers in the spreading water film.

Fig. 6. shows plots of the computationally obtained temporal evolution of the spatial temperature distribution. The snapshots are taken for the case with the power-law velocity profile at times t = 0.04, 0.042, 0.044, 0.046, 0.048, 0.05 μs, ordered from top to bottom in two columns. The temperature continuously decreases as heat is being removed from the wall surface before reaching the steady state. A zoomed detail of the water film spreading over the wall at t = 0.05 μs shows the developing thermal boundary layer within the film of the small thickness, the height of which increases with the radial distance, in accordance with the previous findings.

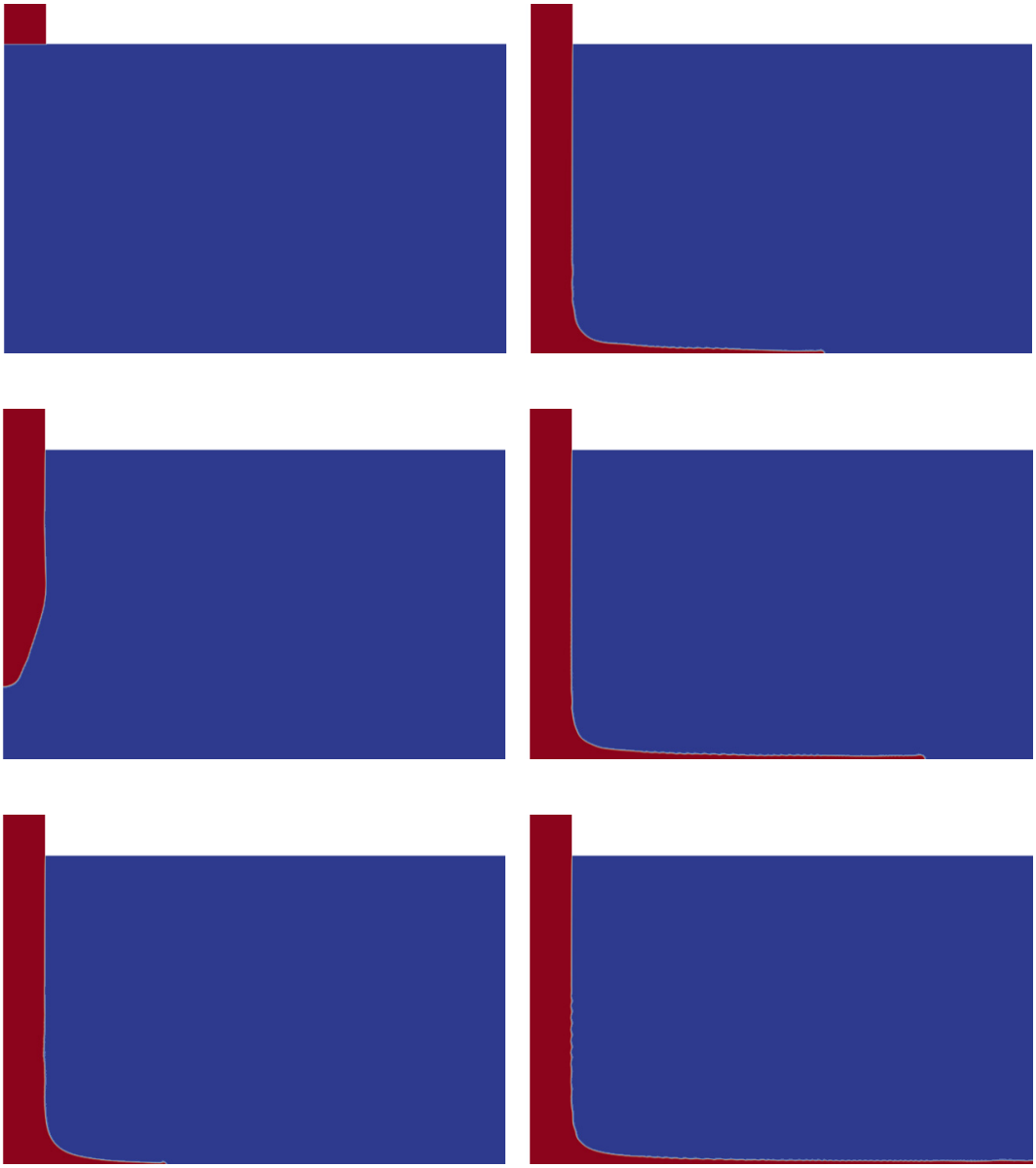

Fig. 5. Temporal evolution of the flow of the impinging jet, snapshots at times t = 0, 0.004, 0.008, 0.012, 0.016, 0.022 μs.

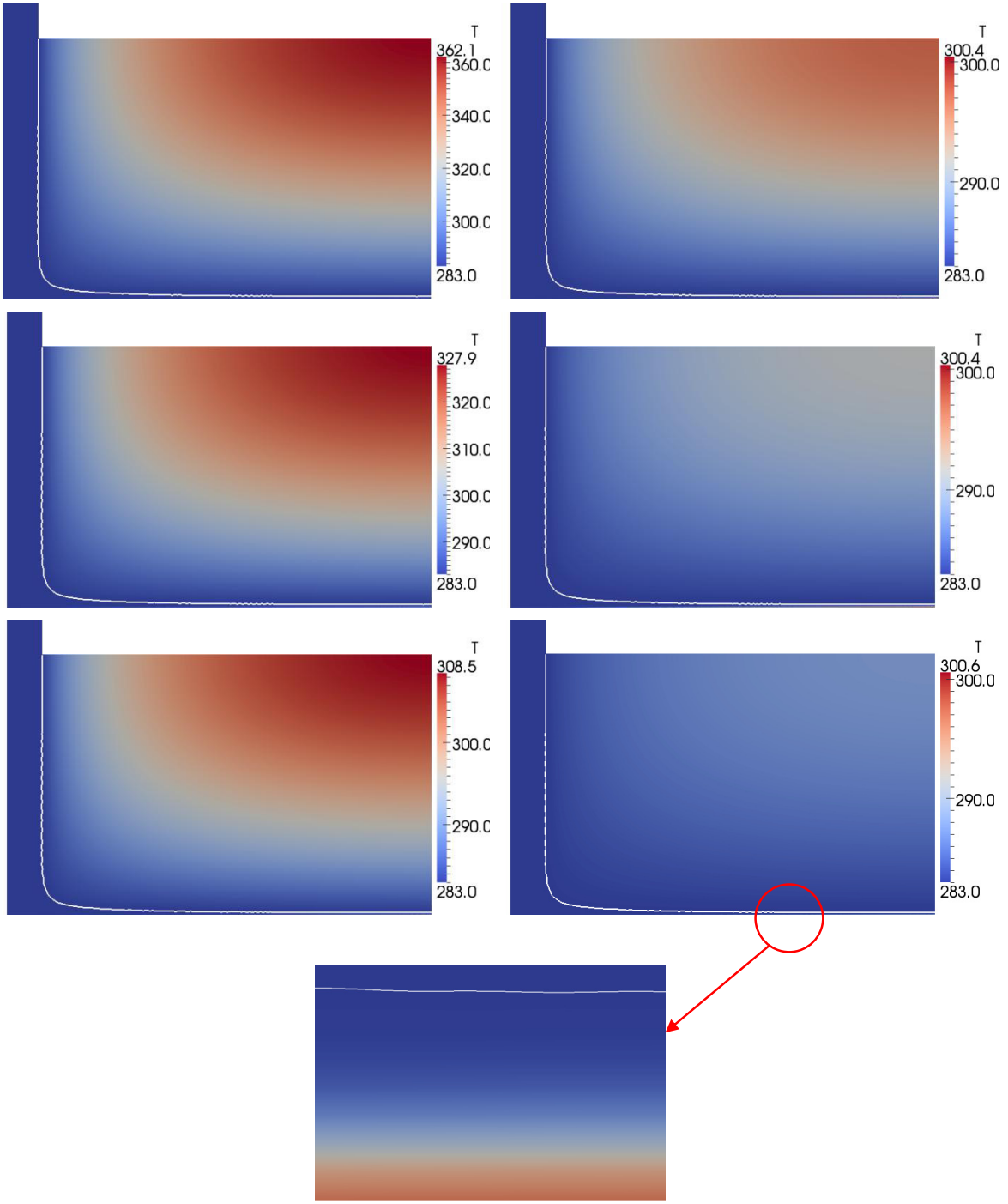

Fig. 6. Temporal evolution of the spatial temperature distribution, snapshots at times t = 0.04, 0.042, 0.044, 0.046, 0.048, 0.05 μs.

Conclusion

The computational model for nonisothermal two-phase flow with free-surfaces is formulated and validated. The model includes the interface capturing methodology based on the volume-of-fluid (VOF) model extended by the energy equation in the form of the temperature equation to enable heat transfer. The smearing of the free surface due to numerical diffusion as the main problem of all numerical interface capturing methodologies is successfully overcome in the present model by the introduction of the additional convective term in the phase fraction governing equation. This term is active only in cells surrounding the free surface and does not alter the overall solution acting as a counter-gradient transport by controlled introduction of downwind effects supressing the numerical diffusion. The temperature equation is implemented to account for the heat exchanged between the boundaries and the computational domain, as well as across the free surface between the two phases. The flow and energy equations are solved in a coupled fashion iterating the fluid motion and the energy equation. The model is validated using numerical simulations of the flow of the liquid jet impacting on a heated wall generating heat transfer from the wall as a common test case. The potential of the computational model is evaluated by comparing the numerically obtained results to the existing experimental, numerical and theoretical results. The results of the computed flow configurations are indicated by the free-surface position, the pressure distribution along the wall surface and the Nusselt number distribution at the wall showing a good agreement with the previously reported results. Some discrepancy in the results for the Nusselt number is observed in the impact region which may be attributed to the fact that the flow was considered as being laminar while in reality some turbulent motions with high velocity gradients may be expected influencing the overall heat transfer coefficient. The computational model can be used for future numerical research to calculate temporal development of the flow and the spatial temperature distribution enabling a detailed insight in the flow and the analysis of heat transfer characteristics of two-phase flows with free-surfaces. Future work includes further improvements of the model to enable conjugate heat transfer and extensions towards problems involving phase changes.

Acknowledgements

The authors would like to thank the Department for Fluid Mechanics and Aerodynamics at the Technical University of Darmstadt, for providing the research facilities required to conduct this research and the German Academic Exchange Service (DAAD) for its support through the research scholarship.

References

[1] Š Šikalo, N. Delalić, E.N. Ganić, Hydrodynamics and heat transfer investigation of air–water dispersed flow, Exp Therm Fluid Sci. 25 (2002) 511-521.
[2] C.W. Hirt, B.D. Nichols, Volume of fluid (VOF) method for the dynamics of free boundaries, J. Comput Phys. 39 (1981) 201-225.
[3] Y. Guo, L. Wei, G. Liang, S. Shen, Simulation of droplet impact on liquid film with CLSVOF, Int. Commun. Heat Mass Transfer 53 (2014) 26-33.
[4] I. Chakraborty, G. Biswas, P.S. Ghoshdastidar, A coupled level-set and volume-of-fluid method for the buoyant rise of gas bubbles in liquids, Int. J. Heat Mass Transfer 58 (2013) 240-259.
[5] M.F. Trujillo, S.R. Lewis, Thermal boundary layer analysis corresponding to droplet train impingement, Phys. Fluids 24 (2012) 112102.
[6] C. Inoue; T. Watanabe; T. Himeno, Atomization and Flow Characteristics of Liquid Sheet Produced by Jet Impingement, J. Propul. Power 28 (2012) 1060-1070.
[7] J.Z. Zhang, X.M. Tan, B. Liu, X.D. Zhu, Investigation for convective heat transfer on grinding work-piece surface subjected to an impinging jet, Appl. Therm. Eng. 51 (2013) 653-661.
[8] R. Scardovelli, S. Zaleski, Interface reconstruction with least-square fit and split Eulerian-Lagrangian advection, Int. J Numer. Meth. Fluids 41 (2003) 251-274.
[9] E. Aulisa, S. Manservisi, R. Scardovelli, S. Zaleski, Interface reconstruction with least-squares fit and split advection in three-dimensional Cartesian geometry, J. Comput. Physics 225 (2007) 2301-2319.
[10] J. Lopez, J. Hernandez, P. Gomez, F. Faura, A volume of fluid method based on multidimensional advection and spline interface reconstruction, J. Comput. Physics 195 (2004) 718-742.
[11] J.E. Pillioid, E.G. Puckett, Second-order accurate volume-of-fluid algorithms for tracking material interfaces, J. Comput. Physics 199 (2004) 465-502.
[12] T. Waclawczyk, T. Koronowicz, Comparison of CICSAM and HRIC high-resolution schemes for interface capturing, J. Theor. Applied Mech. 42 (2008) 325-345.

[13] E. Berberović, N.P. van Hinsberg, S. Jakirlić, I.V. Roisman, C. Tropea, Drop impact onto a liquid layer of finite thickness: Dynamics of the cavity evolution, Phys Rev E 79 (2009) 036306.
[14] J.U. Brackbill, D.B. Kothe, C. Zemach, A continuum method for modeling surface tension, J. Comput Phys. 100 (1992) 335-354.
[15] F.R.S. Batchelor, An Introduction to Fluid Mechanics, Cambridge Universty Press, Cambridge, 1970.
[16] F.P. Incropera, D.P. deWitt, Fundamentals of heat and mass transfer, John Wiley and Sons, New York, 2002.
[17] H. Jasak, OpenFOAM: Open source CFD in research and industry, Inter J. Nav Archit Oc Engng 1 (2009) 89-94
[18] H. Ahmed, S. Chacko, Computational Optimization of Vehicle Aerodynamics, Proc. 23rd Int. DAAAM Symposium, (2012) 0313-0318.
[19] P. Kacor, S. Misak, L. Prokop, Modification of Construction Design of Vertical Axis Wind Turbine, Proc. 22nd Int. DAAAM Symposium (2011) 0723-0724.
[20] B. van Leer, Towards the ultimate conservative difference scheme II. Monotonicity and conservation combined in a second order scheme, J. Comput Phys. 14 (1974) 361-370.
[21] R.I. Issa, Solution of the implicitly discretised fluid flow equations by operator-splitting, J. Comput Phys. 62 (1986) 40-65.
[22] X. Liu, J.H.V. Lienhard, J.S. Lombara, Convective heat transfer by impingement of circular liquid jets, J. Heat Trans-T ASME 113 (1991) 571-582.
[23] H. Fujimoto, N. Hatta, R. Viskanta, Numerical simulation of convective heat transfer to a radial free surface jet impinging on a hot solid, Heat Mass Transfer 35 (1999) 266-272.
[24] A.Y. Tong, A numerical study on the hydrodynamics and heat transfer of a circular liquid jet impinging onto a surface, Numer Heat Tr A-Appl 44 (2004) 11-19.
[25] J. Stevens, Measurements of local heat transfer coefficients: Results for an axisymmetric, single-phase water jet impinging normally on a flat plate with uniform heat flux. Master's thesis, Brigham Young University, Provo, Utah, 1988.